Sensors & Actuators: B. Chemical 305 (2020) 127516

Contents lists available at ScienceDirect

Sensors and Actuators B: Chemical

journal homepage: www.elsevier.com/locate/snb

A low-cost nanomaterial-based electrochemical immunosensor on paper for high-sensitivity early detection of pancreatic cancer

K. Sudhakara Prasad[a], Xiyue Cao[a,b], Ning Gao[a], Qijie Jin[a,c], Sharma T. Sanjay[a], Gilberto Henao-Pabon[d], XiuJun Li[a,d,*]

[a] Department of Chemistry & Biochemistry, University of Texas at El Paso, Texas, USA
[b] College of Chemistry and Chemical Engineering, Qingdao University, Qingdao, 266071, PR China
[c] College of Materials Science and Engineering, Nanjing Tech University, Nanjing 210009, PR China
[d] Biomedical Engineering, Border Biomedical Research Center, and Environmental Science & Engineering, University of Texas at El Paso, USA

ARTICLE INFO

Keywords:
electrochemical biosensor
paper-based microfluidic devices
graphene oxide
pancreatic cancer
PEAK 1
nanomaterial-based immunosensing

ABSTRACT

Due to the lack of specific early detection methods for pancreatic cancer, it usually goes undetected until it is advanced. By employing paper-based electrodes (PPEs), herein we for the first time developed a disposable low-cost paper-based immunosensor for rapid early quantitative detection of pancreatic cancer with a new biomarker, pseudopodium-enriched atypical kinase one, SGK269 (PEAK1). The immunosensor was constructed by fabricating PPEs immobilized with the versatile nanomaterial graphene oxide for the incorporation of antibodies to form an immunosensing platform, without the need of complicated surface modification. After it was confirmed that the PPEs exhibited excellent electrochemical properties, a sandwich-type electrochemical immunosensor was subsequently constructed by employing graphene oxide layers immobilized with anti-PEAK1, and the antibody conjugated with gold nanoparticles (AuNPs-tagged-Anti PEAK1). Further, spectral and surface characteristic studies confirmed the formation of the immunosensing platform. The immunosensor for PEAK1 exhibited a wide linear range between 10 pg mL^{-1} and 10^6 pg mL^{-1} with a low limit of detection (LOD) of 10 pg mL^{-1}. The obtained results point towards rapid, sensitive, and specific early diagnosis of pancreatic cancer at the point of care and other low-resource settings.

1. Introduction

Pancreatic cancer is a malignant neoplasm originating from transformed cells arising in tissues forming the pancreas [1]. It has been reported that pancreatic ductal adenocarcinoma (PDAC) is the fourth leading cancer killer in the United States, even though it is a relatively rare tumor (2% of all cancer cases) [2]. In 2014, it was estimated that there were 46,420 new diagnoses of PDAC and 39,590 deaths attributed to PDAC in the same period [1]. The new cancer statistics also show that the death due to PDAC is far more common than that of breast cancer [3]. In addition, PDAC is projected to become the second leading cause of death by 2030 [4].

As per the scientific framework for PDAC [5], patients diagnosed at the early stage have better long-term survival, but there are no known screening methods to identify the early stage of the carcinogenic process. PDAC may go undetected until it is advanced. When symptoms occur, diagnosis of PDAC is relatively straightforward by using conventional methods such as computed tomography (CT) scan, endoscopic ultrasonography, endoscopic retrograde cholangiopancreatography (ERCP), and magnetic resonance imaging (MRI) [6]. But only a biopsy can finally diagnose PDAC. The biopsy from pancreatic tissues, however, is highly invasive. What's worse, a cure is rarely possible at that moment. Although those traditional diagnostic methods can help determine PDAC, they are costly and generally fail to detect pancreatic cancer at the early stage. A consequence for the late manifestation of symptoms and late diagnosis decreases the five-year survival rate to approximately 5%. Therefore, a simple, low-cost, highly sensitive and specific method is in great demand for the early diagnosis of PDAC. Recently, a tyrosine kinase, PEAK1, was discovered to be up-regulated in human malignancies in human PDACs [7]. The study showed that there were no significant changes in PEAK1 mRNA levels observed between normal and malignant tissues for bladder, head and neck, lung, and so on. Interestingly, a specific increase in PEAK1 protein expression was observed in PDAC tissues in comparison with normal tissues. More recent studies further provided evidence that the KRAS-eIF5A-PEAK1 signaling pathway played a critical role in regulating pancreatic cancer

* Corresponding author at: Department of Chemistry & Biochemistry, University of Texas at El Paso, Texas, USA.
E-mail address: xli4@utep.edu (X. Li).

https://doi.org/10.1016/j.snb.2019.127516
Received 8 April 2019; Received in revised form 28 November 2019; Accepted 30 November 2019
Available online 02 December 2019
0925-4005/

cell proliferation, migration, and metastasis [8]. Thus, PEAK1 is regarded as a novel biomarker, critical signaling hub, and new therapeutic target for PDAC. Currently, conventional methods for PEAK measurement is mainly based on tissue immunohistochemistry and western blot [7,8]. Both techniques are invasive, cumbersome, and they can only provide semi-quantitative results.

A number of conventional immunoassay methods such as enzyme-linked immunosorbent assay (ELISA), radioimmunoassay, fluorescent immunoassay, chemiluminescence immunoassay, electrophoretic immunoassay, and mass spectrometry-based proteomics have been established during the past decades for quantitative biomarker detection [9–16]. Even though most of these methods are highly selective and sensitive, they are costly, require extensive time to carry out, have a complicated sample pre-treatment, and the use of sophisticated instruments. Sometimes a low concentration of a cancer biomarker (particularly less than 1 ng/mL) in the early stages of cancer is undetectable during ELISA. On the other hand, electrochemical immunoassay [17–19], mainly based on the electrochemical detection of the labeled immunoagents or markers such as enzymes, metal nanoparticles, or other electroactive compounds showed enhanced detection sensitivity. Among electrochemical immunoassays, paper-based electrochemical detection is much simpler, cost effective, and easier to achieve with less complex fabrication procedures [20,21].

Previously, electrochemical detection by employing paper-based microfluidic devices was demonstrated by Dungchai et al. [22] and has been used for the detection of biomolecules such as glucose, lactate, and uric acid. Nie et al. [23] reported an electrochemical sensing method in paper-based microfluidic devices for the detection of heavy metal ions and glucose. In addition, Li et al. [20] reported the first paper-based electrochemical ELISA with low assay time, high sensitivity, and low LOD in the femtomole range for IgG. After the invention of paper electrochemical ELISA, there is a tremendous growth of research reports about the electrochemical paper-based assay for sensing proteins, biomarkers, and other biologically important molecules, emphasizing the advantages of paper-based electrochemical immunoassay methods [24–28]. In addition, paper-based microfluidic devices incorporated the advantages of both microfluidics [29–34] (e.g. portability, minimal sample consumption, and rapid detection) and paper-based electrochemical sensors (e.g. printable, impregnable and inexpensive manufacturability from renewable and reusable resources) [25,35], and have been recognized as a low-cost and disposable sensing platforms [10,33,36–44].

Herein, for the first time, we report a simple, disposable, low-cost, yet novel electrochemical immunosensor on paper for the trace determination of the PDAC biomarker PEAK1 through a traditional sandwich-type immunoassay. The electrochemical immunosensing platform was developed on a PPE, which was fabricated using the manual screen printing technique [22]. Further, graphene oxide, a 2D nanomaterial [45], was simply dropped cast onto PPE for the incorporation of capture antibody (Anti-PEAK1) through a covalent modification procedure. The immunosensing platform utilized gold nanoparticle (AuNPs)-tagged Anti-PEAK1 bioprobes for the detection of PEAK1. During the fabrication process, the immunosensor probes were characterized by spectral, surface morphological, and electrochemical studies. By applying the differential pulse voltammetry technique, the developed sensor was demonstrated to exhibit a high sensitivity in monitoring PEAK1 with a LOD of 10 pg/mL, showing tremendous potential for early detection of pancreatic cancer. To the best of our knowledge, such a low-cost and specific PEAK1 immunosensor has not been reported for the early quantitative diagnosis of PDAC.

2. Materials and method

2.1. Materials and apparatus

Potassium ferricyanide ($K_3Fe(CN)_6$) (ACS grade) was obtained from Fisher, while 1-ethyl-3[dimethylaminopropyl] carbodiimide hydrochloride (EDC), N-hydroxysuccinimide (NHS), gold nanoparticle (AuNPs) with a 20 nM diameter, bovine serum albumin (BSA), chromatography paper (Whatman 1 chr), and all other chemicals were purchased from Sigma-Aldrich. A pH 7.4 phosphate buffer solution (PBS) was used in all studies. Graphene oxide (GO, carbon 79% and oxygen 20%) was purchased from Graphene Laboratories (Calverton, NY). PEAK1 recombinant protein, carcinoembryonic antigen (CEA), and anti-PEAK1 were obtained from MyBiosource Inc (San Diego, CA). Deionized water (> 18 MΩ·cm) from a Millipore purification system was used to prepare all aqueous solutions. Conductive carbon and Ag/AgCl ink were procured from Conductive Compounds Inc. (Houston, TX), to develop carbon-based working electrodes (WE), and counter electrodes (CE) and silver pseudo reference electrodes (RE).

Voltammetric measurements were carried out with a CH Instrument (CHI 730E, Austin, TX) electrochemical workstation. UV–vis spectra were recorded with a BMG SPECTRO star Nano Plate Reader. The FT-IR spectrum was recorded by using Spectrum 100 FT-IR Spectrometer, Perkin Elmer [46]. Transmission electron microscopy (TEM) images were obtained from JEOL JEM 3200 FS. X-ray photoelectron spectroscopy (XPS) analysis was conducted by using PHI 5000 Versa Probe X-ray photoelectron spectrometer (Physical Electronics) and curve fitting was performed with XPSPEAK41 system software.

2.2. Fabrication of paper electrodes

Paper-based electrodes (PPEs) were first designed by the Adobe Illustrator graphic design software and fabricated using the stencil-printing technique that was previously reported by Nie et al. [23]. Briefly, a stencil-printing mask with the electrode pattern on it was created by laser-cutting low-tack frisket films with an in-house laser cutter Zing 16 (Epilog, Golden, CO). The as-developed electrode patterns were then placed onto the SU-8 2010 photo resist-treated chromatographic paper, which was pre-prepared using the photolithography technique. Next, conductive carbon ink paste was pasted on the electrode patterns to develop a 3-electrode system that consisted of a carbon-based working and counter electrodes, and an Ag/AgCl ink-based pseudo reference electrode. After careful pasting of the ink, the electrodes were then backed at 100 °C for 20 min in an oven. The obtained electrodes were washed with copious amounts of water and dried under a nitrogen stream, and further used for electrochemical studies. Schematic representation of the fabrication procedure is shown in Scheme 1. The as-fabricated PPE has a working electrode surface area of 7.06 mm^2.

2.3. Preparation of AuNPs-tagged-Anti PEAK1 bioprobes

Bioconjugation of AuNPs to Anti PEAK1 was performed through a simple physisorption method. Briefly, AuNPs-tagged-Anti PEAK1 were synthesized by adding 10 μL of 20 μg mL^{-1} Anti PEAK1 in 0.01 M PBS to 100 μL of a 20 nm diameter AuNPs solution in PBS, followed by gentle mixing at 4 °C for 12 h. After mixing and centrifugation, the obtained AuNPs-tagged-Anti PEAK1 was reacted with 0.5% BSA to block any possible remaining active sites to avoid any non-specific absorption. The prepared AuNPs-tagged-Anti PEAK1 bioprobes were stored at 4 °C until use.

2.4. Fabrication of immunosensors

The as-prepared paper electrodes were drop-coated with 3 μL of an aqueous solution of GO (5.5 mg mL^{-1}) and subsequently dried at 65 °C for 15 min., forming the GO-PPE composite. Next, the obtained GO-PPE electrodes were treated with 0.35 M of EDC and 0.1 M of NHS for another 15 min. to activate the –COOH functionalities of GO [46,47]. After the activation process, the modified electrodes Anti PEAK1 (20 μg mL^{-1} in PBS) was immediately incubated with Anti PEAK1 (20 μg

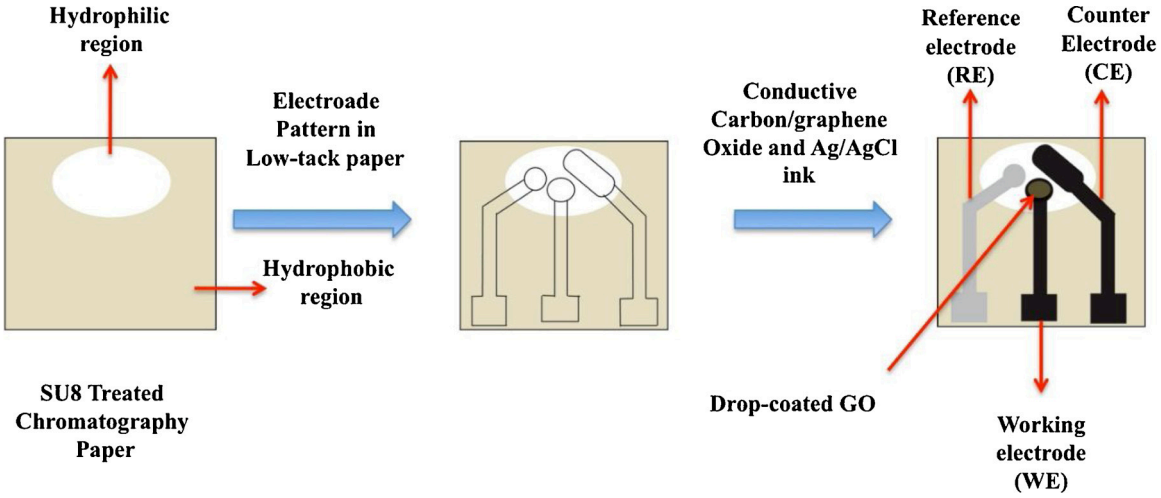

Scheme 1. Schematic representation of the fabrication process of the disposable paper-based electrode (Pictures not drawn to scale).

mL^{-1} in PBS) at 4 °C for 60 min. to obtain Anti PEAK1-GO-PPE. After washing, 0.5% BSA was added for 15 min. to block nonspecific binding sites. Then, different concentrations of PEAK 1 samples were introduced to the modified electrodes, incubating for 30 min. at 4 °C to allow the immuno-recognition. After rinsing with PBS again to remove the unbound PEAK1, AuNPs-tagged-Anti PEAK1 was incubated for 45 min at 4 °C to form sandwich immuno-complexes. Finally, the unbound AuNPs bioconjugates were washed off with PBS and subsequently used for electrochemical and surface morphological studies.

2.5. Electrochemical measurements

Electrochemical measurements were carried out using a CHI electrochemical workstation with a 3-electrode paper-based microfluidic device. Differential pulse voltammetry (DPV) was performed to characterize the modified electrodes to achieve its high signal to noise ratio because DPV is more sensitive to oxidation or reduction current (faradaic current) than conventional DC voltammetry. The modified electrodes were characterized by recording the response towards a common redox probe, $K_3Fe(CN)_6$.

3. Results and discussion

3.1. Principle of the paper-based PEAK1 immunosensor

Scheme 2 illustrates the main detection process and principle of the paper-based PEAK1 immunosensor. After paper-based carbon working electrode is prepared, it is drop-coated with a GO solution. Once GO is dried at 65 °C, it forms the GO-PPE composite, in which GO is used as a platform to immobilize antibodies on the electrode. In the presence of EDC and NHS, the PEAK1 antibody is coupled with the GO-PPE electrode for specific recognition of the pancreatic cancer biomarker PEAK1. After washing with BSA, to prevent non-specific binding, PEAK1 and gold nanoparticle-labeled antibodies will be introduced separately, forming a sandwich-structure immunoassay system. The gold particles introduced by the immunoreaction will increase the electroactive area on the GO electrode, and further improve the conductivity and electron transfer of the electrode [48,49]. As a result, a paper-based immunosensor becomes ready for the electrochemical detection of PEAK1 in a typical electrochemical system of potassium ferricyanide.

3.2. Characterization of AuNPs-tagged-Anti PEAK1 bioprobes

We first characterized the as-prepared AuNPs bioconjugate suspension with respect to the naked AuNPs using UV–vis absorption spectroscopy. As shown in Fig. 1, the naked AuNPs depicted a common surface plasmon resonance peak (SPR) at 520.0 nm, consistent with the literature reported SPR peak for 20 nm diameter AuNPs [50]. After the bioconjugation of AuNPs with Anti-PEAK1, the SPR band shifted to 522.8 nm (redshift) as indicated in Fig. 1. This spectral shift is due to the change in AuNPs size or due to the aggregation resulted from the physical adsorption of anti-PEAK1 onto AuNPs, during the bioconjugation process. A similar phenomenon was previously reported when antibodies were conjugated to AuNPs [51]. This spectral shift obviously supports the formation of AuNPs-tagged-Anti PEAK1 bioprobes. Further experimental techniques such as TEM revealed some obvious changes in the structural morphology of AuNPs before and after the addition of Anti-PEAK1 (Fig.1B-C). The obvious aggregation of the AuNPs is observed (Fig. 1C), unlike the individual well separated AuNPs in Fig. 1B. The TEM results further support the formation of AuNPs-tagged-Anti PEAK1 bioprobes.

3.3. Characterization of the immunosensor

The properties of the functionalized immunosensor were characterized by FTIR and XPS. First, the study of ATR-FTIR spectra (Fig. S1) shows typical IR bands at 1038, 1360, 1618, 1740, and 3100 cm^{-1} for C−O, C═C, C═O, and −OH groups from graphene oxide on GO-PPE, and the antibody immobilized anti-PEAK1-GO-PPE exhibited typical IR bands for amide II N−H bonds between 1600 cm^{-1} and 1700 cm^{-1}, and N−H bands at 3168 cm^{-1}, which confirmed successful electrode modification (see Supplementary Information for more details).

Furthermore, the detailed compositional analysis of PPE, GO-PPE, and Anti-PEAK1-GO-PPE was carried out by using XPS. From the XPS survey scan (Fig. 2), the atomic percentages of PPE were derived as 82.4% carbon, 2.5% oxygen, and 2.3% nitrogen. GO-PPE exhibited 67.1% carbon, 31.1% oxygen, and 0.7% nitrogen. When the antibody was immobilized on the electrode, Anti-PEAK1-GO-PPE showed 66.1% for carbon, 27% oxygen and 3.5% nitrogen. The atomic percentages of carbon, oxygen, and nitrogen in the developed immunosensor were found to be 68.3, 18.4 and 12.4%, respectively (Fig. S2). This explains the formation of chemical functionalities based on C, N, and O on the electrode surface. The survey scan for the immunosensor showed some trace amounts of Au for AuNPs and sulfur. In addition, the atomic ratios of O_{1s}/C_{1S} and were calculated to be 0.03% and 0.02% for PPE. On the other hand, an increased ratio of O_{1s}/C_{1S} of 0.46% for GO-PPE indicated the increased amount of oxygen functionalities on the electrode surface, while the N_{1s}/C_{1S} ratio was found to be 0.01%, pointing

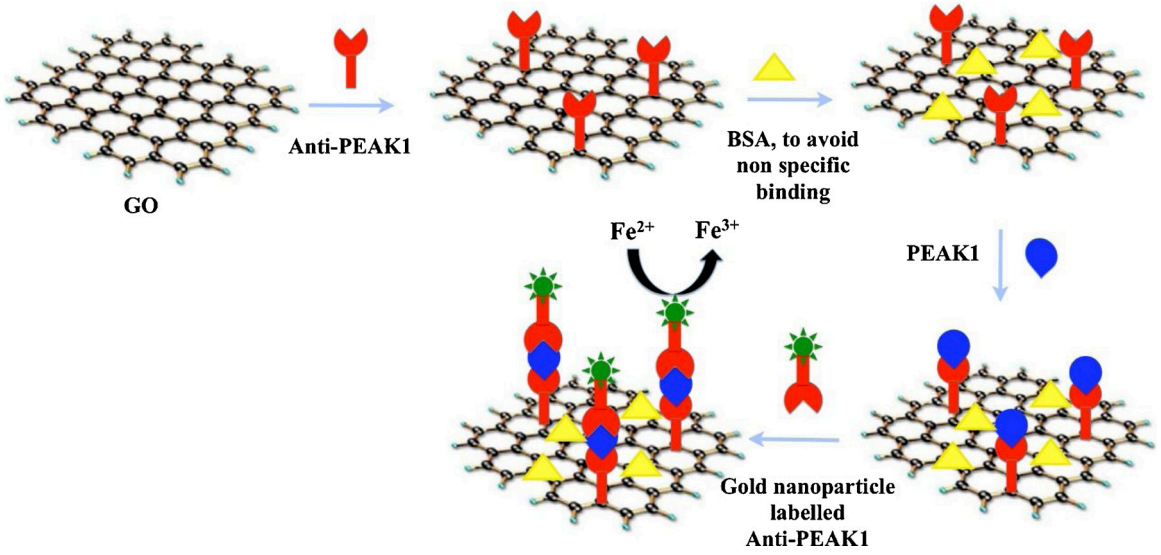

Scheme 2. Schematic representation of the principle of the PEAK1 immunosensor.

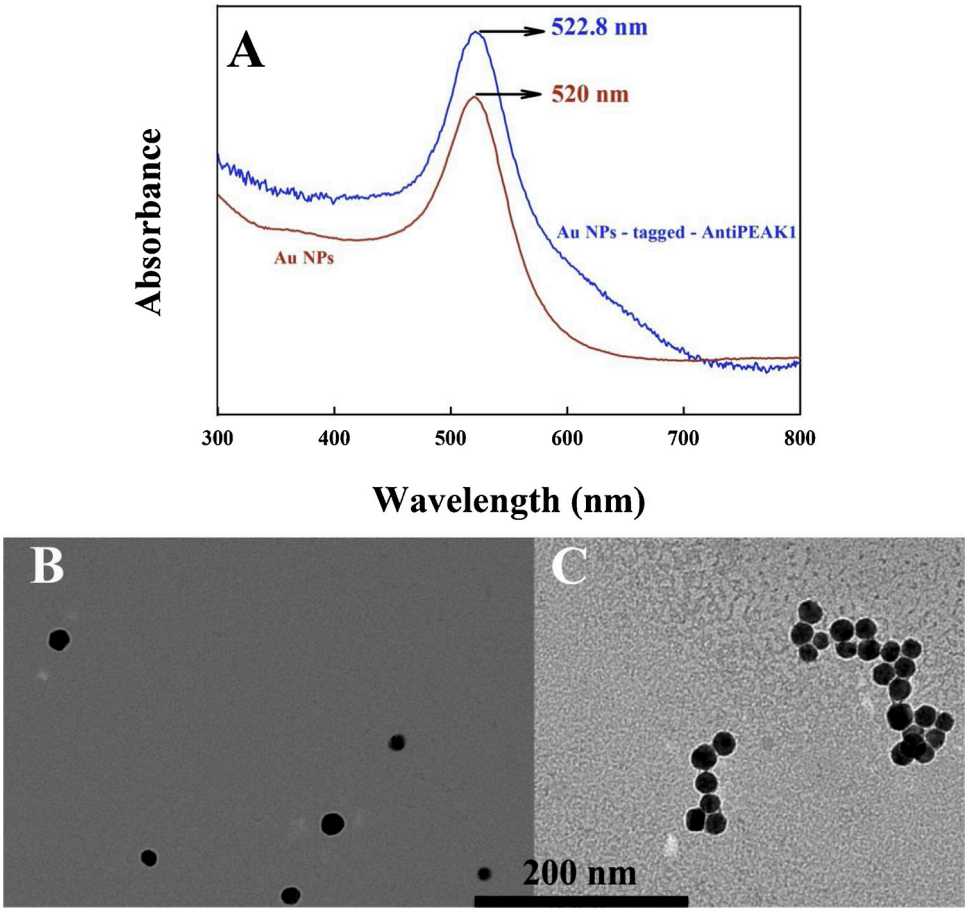

Fig. 1. UV–vis absorption spectra of AuNPs before and after immobilization of Anti PEAK1 (A), and TEM images of the AuNPs (B) before and after (C) the formation of AuNPs-tagged-Anti PEAK1 bioprobes.

towards the negligible presence of nitrogen. As to the case of Anti-PEAK1-GO-PPE, the atomic ratios of O_{1s}/C_{1S} and N_{1s}/C_{1S} were calculated to be 0.40% and 0.05 %, respectively. The former ratio was smaller than the calculated O_{1s}/C_{1S} atomic ratio of GO-PPE, whereas the latter was higher than the N_{1s}/C_{1S} atomic ratio of GO-PPE. The decrease in oxygen functionalities, while with an increase of nitrogen functionalities at Anti-PEAK1-GO-PPE explicitly indicates the immobilization of Anti-PEAK1 on GO. The immunosensor showed a further decrease in the atomic ratio of O_{1s}/C_{1S} (0.26%) and an increase in the N_{1s}/C_{1S} (0.18%) atomic ratio, due to the further addition of PEAK1 proteins and AuNPs-tagged-Anti PEAK1 bioprobes. Additionally, the deconvoluted Au 4f XPS spectra with doublets at 82.5 eV and 86.2 eV for $4f_{5/2}$ and $4f_{7/2}$ for the immunosensor (Fig. S2) revealed the formation of AuNPs-tagged-Anti PEAK1 bioprobes through the

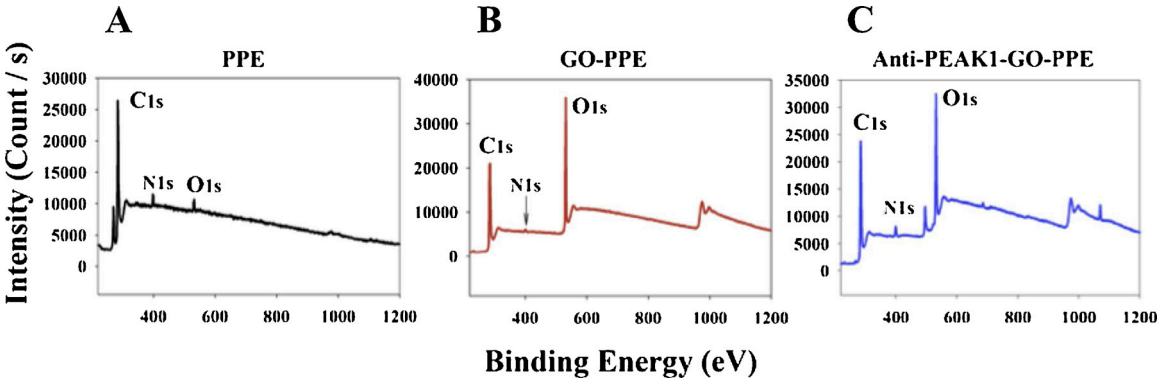

Fig. 2. XPS Survey Scan for PPE, GO-PPE, and Anti-PEAK1-GO-PPE.

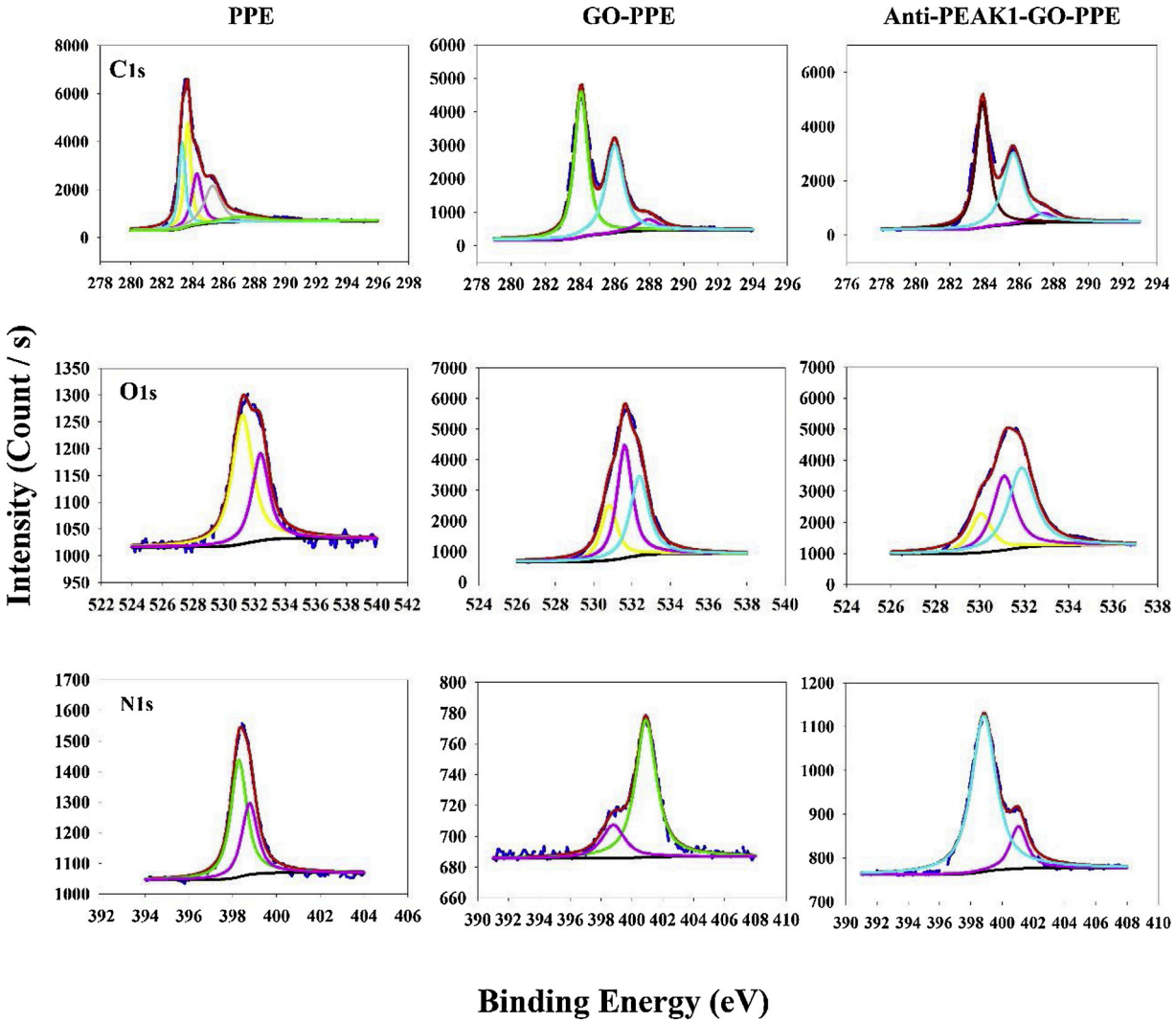

Fig. 3. Deconvoluted C_{1S}, O_{1s}, and N_{1s} XPS spectra for PPE, GO-PPE, and Anti PEAK1-GO-PPE.

binding of AuNPs with -NH_2 functionalities of Anti-PEAK1 via pseudo-covalent fashion [52]. See SI for a more detailed discussion.

Moreover, the deconvoluted XPS spectra (Fig. 3) binding energy values (Table S1) reveal more information about the chemical bond formation and surface functionalities involved during the development of the PEAK1 immunosensor. The new peaks (287.9 eV and 287.4 eV) in the C_{1S} spectra showed that the O—C = O and N—C = O bonds existed in the GO-PPE and Anti-PEAK1-GO-PPE, respectively. The results indicated that GO was immobilized on the electrode surface and the Anti-PEAK1 was also formed on the GO-PPE surface. From the O_{1S} spectra, the most obvious change was the increase in peak intensity, which was attributed to the modification of GO. The peak intensities in the N_{1S} spectra followed the order: PPE > Anti-PEAK1-GO-PPE > GO-PPE. It was mainly because of the change of relative amounts of the N element in different samples after the addition of GO and Anti-PEAK1. Taken together, the aforementioned spectral and XPS studies clearly indicate the formulation process of the PEAK1 immunosensor on PPE.

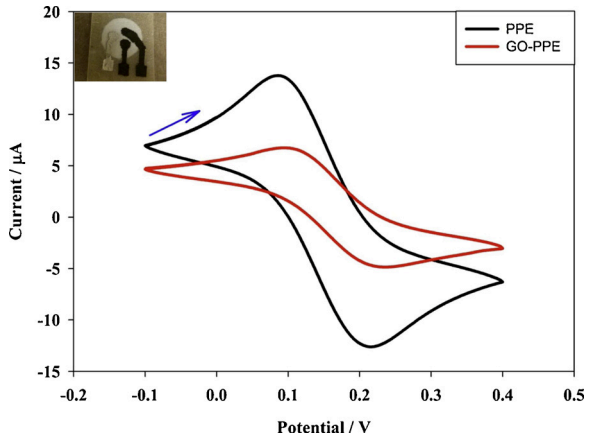

Fig. 4. Cyclic voltammograms of PPE and GO-PPE in 5 mM $K_3Fe(CN)_6$ in 0.1 M KCl solutions at a scan rate of 50 mV/s, and the inset depicts the fabricated PPE.

3.4. Electrochemical characteristics of modified electrodes

As discussed in the experimental section, PPEs were used to develop the immunosensor for PEAK1 detection. Hence, their electrochemical characteristics were first investigated before testing the immunosensor. Fig. 4 depicts the CV studies of the fabricated PPE with common benchmark redox couple $K_3Fe(CN)_6$, which exhibited distinct redox peaks for the oxidation and reduction of ferricyanide. Notably, after the drop coating of GO onto PPE, there was a decrease in the redox peak current, which was attributed to the poor electron transfer ability of GO. The electrochemical characterization of the electrodes was further studied by running DPV in a 5 mM $K_3Fe(CN)_6$ solution prepared in 0.1 M KCl. The DPV of modified electrodes with respect to the unmodified one showed a substantial decrease in the peak current in Fig. S3. The DPV profiles for PPE showed a well-defined peak with higher current, which was attributed to the prominent electron transferability of the as-prepared PPE. On the other hand, GO modified electrodes exhibited a voltammogram (curve b) with less current, due to the poor electron transfer ability of GO (decorated mostly with carboxyl functionalities) towards an anionic redox probe such as $K_3Fe(CN)_6$, due to the repulsive electrostatic interaction between the anionic probe and negatively charged GO. A similar trend of a decrease in the peak current for Anti-PEAK1 (curve c) was observed as in the case of GO-PPE. This phenomenon might be due to the protein fouling effect caused by the immobilized antibodies or the repulsive electrostatic interactions between the negatively charged antibody molecules at values of pH greater than its isoelectronic point, which facilitates an insulating barrier that delays the electron transfer at electrodes. The decrease in peak current suggests that the GO and Anti-PEAK1 were successfully immobilized on PPE.

3.5. Analytical performance of the immunosensor

The analytical performance of the immunosensor was investigated using DPV towards different concentrations of PEAK1, by at least triplicate experiments at each concentration. As shown in Fig. 5A–C, an increase in the concentration of PEAK1 during immunorecognition resulted in more Au bioprobes binding to the captured PEAK1, leading to an increment in the DPV peak current. The detailed analysis of the immunosensor response towards PEAK1 reveals a linear increase in the DPV current with respect to different logarithmic concentrations of PEAK1 in the range of 10 pg mL^{-1} to 10^6 pg mL^{-1} (Fig. 5C). The LOD was calculated to be 10 pg mL^{-1} from the concentration-dependent curve by adding three times the standard deviation of the blank or control from its average value, indicating high detection sensitivity of the paper-based electrochemical immunosensor. The reproducibility of the proposed PEAK1 immunosensor was evaluated through the analysis of three independent immunosensors strips. The current response for 10 pg mL^{-1} PEAK1 gave a relative standard deviation (RSD.) of 3.08%, which indicated good reproducibility and precision of the immunosensor.

To validate the biosensor, we further tested human serum samples spiked with different concentrations of standard PEAK1. As listed in Table 1, all the recovery values in serum sample testing were determined at the satisfactory level ranging from 103 to 104%, with RSDs from 2.37 to 2.97%. In addition, we investigated the specificity of the biosensor. Some common interfering substances including a common cancer biomarker, carcinoembryonic antigen (CEA) [53], and BSA were tested using paper-based electrochemical biosensor. A significant current increase of 9.5 µA was monitored for the target PEAK1 (100.0 ng/mL), while CEA and BSA only showed similar responses to the blank sample, as shown in Fig. S4, indicating high specificity of the electrochemical biosensor mainly due to the high specificity from immunoassays.

4. Conclusions

We have developed a simple, low-cost, disposable paper-based electrochemical immunosensor for quantitative early detection of the pancreatic cancer biomarker PEAK1. It reveals that the PPE electrode surface is suitable for the covalent grafting of bio-reagents through a graphene oxide modification procedure. Further surface characteristic studies such as FT-IR and XPS confirmed the immobilization of Anti-PEAK1 on GO-PPEs and the formation of the immuosensor probe for PEAK1. The disposable PEAK1 electrochemical immunosensor exhibited a low detection limit of 10 pg mL^{-1} in physiological pH solutions with a logarithmic linear response up to 10^6 pg mL^{-1}. Current methods for PEAK measurement are mainly based on tissue immunohistochemistry and western blot. Because both techniques are invasive, cumbersome, and can only provide semi-quantitative results, which is more likely to be used for the diagnosis of late-stage cancers. This work provides a simple and low-cost paper-based electrochemical immunosensor for rapid, sensitive, and quantitative early diagnosis of pancreatic cancer. To the best of our knowledge, this is the first low-cost biosensor for sensitive and quantitative PEAK1 detection in a less invasive fashion. The immunosensor does not need any enzyme which can degrade quickly at room temperature, and thus makes the paper-based imumunosensor more robust at room temperature. The gold nanoparticles-based electrochemical sensor has tremendous potential for dual detection: that is, color changes from AuNPs can be used for visual qualitative detection by the naked eye, while the electrochemical detection provides more sensitive and quantitative data. On the other hand, by incorporating more microfluidic reaction zones and microchannels and nanosensors [54–57], the as-developed paper-based electrochemical immunosensing platform will have great potential for multiplexed measurement of various biomarkers for affordable point-of-care diagnostics [58–60], especially for resource-limited settings such as developing countries.

Declaration of Competing Interest

The authors declare that they have no known competing financial interests or personal relationships that could have appeared to influence the work reported in this paper.

Acknowledgment

We are grateful to the financial support from the National Institute of Allergy and Infectious Disease of the NIH (R21AI107415), the Philadelphia Foundation, the Medical Center of the Americas Foundation, and the U.S. NSF-PREM program (DMR 1827745). Financial support from the National Institute of General Medical Sciences of the NIH (SC2GM105584), the NIH RCMI Pilot grant

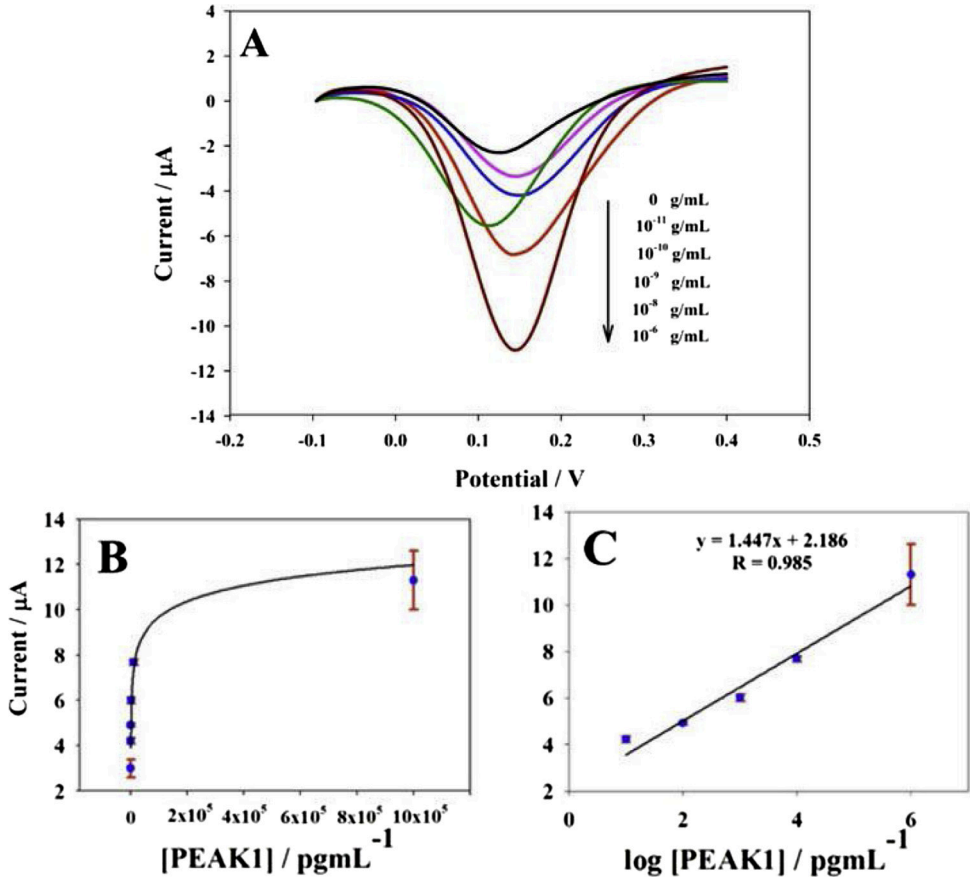

Fig. 5. (A) DPV profile for electrochemical immunosensing of different concentrations of PEAK1. (B) Measured DPV current at different PEAK1 concentrations. (C) Calibration curve versus the logarithm of the PSA concentration. Error bar represents the standard deviation across three repeated measurements.

Table 1
Measurement of PEAK1 in spiked human serum samples (n = 3).

Spiked Concentration (ng/mL)	Measured Concentration (ng/mL)	RSD (%)	Recovery (%)
10.0	10.4	2.37	104
40.0	41.2	2.97	103

(5G12MD007593-22), University of Texas (UT) System for the STARS award, and the University of Texas at El Paso (UTEP) for the IDR Program is also greatly acknowledged.

Appendix A. Supplementary data

Supplementary material related to this article can be found, in the online version, at doi:https://doi.org/10.1016/j.snb.2019.127516.

References

[1] A. Stark, G. Eibl, Pancreatic ductal adenocarcinoma, Pancreapedia: The Exocrine Pancreas Knowledge Base, (2015).
[2] I. Grantzdorffer, S. Carl-McGrath, M.P. Ebert, C. Rocken, Proteomics of pancreatic cancer, Pancreas 36 (May) (2008) 329–336.
[3] R.L. Siegel, K.D. Miller, A. Jemal, Cancer statistics, 2016, CA Cancer J. Clin. 66 (January-Febuary) (2016) 7–30.
[4] L. Rahib, B.D. Smith, R. Aizenberg, A.B. Rosenzweig, J.M. Fleshman, L.M. Matrisian, Projecting cancer incidence and deaths to 2030: the unexpected burden of thyroid, liver, and pancreas cancers in the United States, Cancer Res. 74 (June 1) (2014) 2913–2921.
[5] N. C. Institute, ed, 2014.
[6] M. Hidalgo, Pancreatic cancer, N. Engl. J. Med. 362 (April 29) (2010) 1605–1617.
[7] J.A. Kelber, T. Reno, S. Kaushal, C. Metildi, T. Wright, K. Stoletov, et al., KRas induces a Src/PEAK1/ErbB2 kinase amplification loop that drives metastatic growth and therapy resistance in pancreatic Cancer, Cancer Res. 72 (2012) 2554–2564.
[8] J. Strnadel, S. Choi, K. Fujimura, H. Wang, W. Zhang, M. Wyse, et al., eIF5A-PEAK1 signaling regulates YAP1/TAZ protein expression and pancreatic Cancer cell growth, Cancer Res. 77 (April 15) (2017) 1997–2007.
[9] S. Lai, S. Wang, J. Luo, L.J. Lee, S.T. Yang, M.J. Madou, Design of a compact disk-like microfluidic platform for enzyme-linked immunosorbent assay, Anal. Chem. 76 (April 1) (2004) 1832–1837.
[10] S.T. Sanjay, M. Dou, J. Sun, X. Li, A paper/polymer hybrid microfluidic microplate for rapid quantitative detection of multiple disease biomarkers, Sci Rep, vol. 6 (July 26) (2016) 30474.
[11] W.T. Al-Jamal, K.T. Al-Jamal, P.H. Bomans, P.M. Frederik, K. Kostarelos, Functionalized-quantum-dot-liposome hybrids as multimodal nanoparticles for cancer, Small 4 (September) (2008) 1406–1415.
[12] Z. Fu, F. Yan, H. Liu, J. Lin, H. Ju, A channel-resolved approach coupled with magnet-captured technique for multianalyte chemiluminescent immunoassay, Biosens. Bioelectron. 23 (May 15) (2008) 1422–1428.
[13] Y.J. Ko, J.H. Maeng, Y. Ahn, S.Y. Hwang, N.G. Cho, S.H. Lee, Microchip-based multiplex electro-immunosensing system for the detection of cancer biomarkers, Electrophoresis 29 (August) (2008) 3466–3476.
[14] S. Hu, S. Zhang, Z. Hu, Z. Xing, X. Zhang, Detection of multiple proteins on one spot by laser ablation inductively coupled plasma mass spectrometry and application to immuno- microarray with element-tagged antibodies, Anal. Chem. 79 (Febuary 1) (2007) 923–929.
[15] E.E. Niederkofler, K.A. Tubbs, K. Gruber, D. Nedelkov, U.A. Kiernan, P. Williams, et al., Determination of beta-2 microglobulin levels in plasma using a high-throughput mass spectrometric immunoassay system, Anal. Chem. 73 (July 15) (2001) 3294–3299.
[16] K. Saito, D. Kobayashi, M. Sasaki, H. Araake, T. Kida, A. Yagihashi, et al., Detection of human serum tumor necrosis factor-alpha in healthy donors, using a highly sensitive immuno-PCR assay, Clin. Chem. 45 (May) (1999) 665–669.
[17] F.S. Felix, L. Angnes, Electrochemical immunosensors - A powerful tool for analytical applications, Biosens. Bioelectron. 102 (April 15) (2018) 470–478.
[18] B.V. Chikkaveeraiah, A.A. Bhirde, N.Y. Morgan, H.S. Eden, X.Y. Chen, Electrochemical immunosensors for detection of Cancer protein biomarkers, ACS Nano 6 (August) (2012) 6546–6561.
[19] A. Warsinke, A. Benkert, F.W. Scheller, Electrochemical immunoassays, Fresenius J. Anal. Chem. 366 (March-April) (2000) 622–634.
[20] H. Chen, X. Li, L. Wang, P.C. Li, A rotating microfluidic array chip for staining assays, Talanta 81 (June 15) (2010) 1203–1208.
[21] X.J. Li, Z.H. Nie, C.-M. Cheng, A.B. Goodale, G.M. Whitesides, Paper-based

electrochemical ELISA, Proc. Micro Total Analysis Systems 14 (2010) 1487–1489.
[22] W. Dungchai, O. Chailapakul, C.S. Henry, Electrochemical detection for paper-based microfluidics, Anal. Chem. 81 (July15) (2009) 5821–5826.
[23] Z. Nie, C.A. Nijhuis, J. Gong, X. Chen, A. Kumachev, A.W. Martinez, et al., Electrochemical sensing in paper-based microfluidic devices, Lab Chip 10 (Febuary 21) (2010) 477–483.
[24] J. Adkins, K. Boehle, C. Henry, Electrochemical paper-based microfluidic devices, Electrophoresis 36 (August) (2015) 1811–1824.
[25] M.W. Dou, S.T. Sanjay, M. Benhabib, F. Xu, X.J. Li, Low-cost bioanalysis on paper-based and its hybrid microfluidic platforms, Talanta 145 (December 1) (2015) 43–54.
[26] J. Mettakoonpitak, K. Boehle, S. Nantaphol, P. Teengam, J.A. Adkins, M. Srisa-Art, et al., Electrochemistry on paper-based analytical devices: a review, Electroanalysis 28 (July) (2016) 1420–1436.
[27] P. Teengam, W. Siangproh, A. Tuantranont, C.S. Henry, T. Vilaivan, O. Chailapakul, Electrochemical paper-based peptide nucleic acid biosensor for detecting human papillomavirus, Anal. Chim. Acta 952 (Febuary 1) (2017) 32–40.
[28] H. Manisha, P.D.P. Shwetha, K.S. Prasad, Low-cost Paper Analytical Devices for Environmental and Biomedical Sensing Applications, Environ. Chem. Med. Sens. (2018) 315–341.
[29] X.J. Li, Y. Zhou, Microfluidic Devices for Biomedical Applications, Woodhead Publishing, 2013.
[30] M. Dou, N. Macias, F. Shen, J. Dien Bard, D.C. Domínguez, X. Li, Rapid and accurate diagnosis of the respiratory disease pertussis on a point-of-Care biochip, E Clin. Med. 8 (2019) 72–77 02/01/ 2019.
[31] S.T. Sanjay, W. Zhou, M. Dou, H. Tavakoli, L. Ma, F. Xu, et al., Recent advances of controlled drug delivery using microfluidic platforms, Adv. Drug Deliv. Rev. 128 (2018) 3–28 (*Five-Year impact factor 17.3), 2018/03/15/.
[32] F. Shen, Y. Li, Z. Liu, X. Li, Study of flow behaviors of droplet merging and splitting in microchannels using Micro-PIV measurement, Microfluid. Nanofluidics 21 (2017) 66.
[33] M. Dou, S.T. Sanjay, D.C. Dominguez, S. Zhan, X. Li, A paper/polymer hybrid CD-like microfluidic SpinChip integrated with DNA-functionalized graphene oxide nanosensors for multiplex qLAMP detection, Chem Comm 53 (2017) 10886–10889.
[34] M. Dou, J.M. Garcia, S. Zhan, X. Li, Interfacial nano-biosensing in microfluidic droplets for high-sensitivity detection of low-solubility molecules, Chem Comm 52 (2016) 3470–3473.
[35] S.T. Sanjay, G.L. Fu, M.W. Dou, F. Xu, R.T. Liu, H. Qi, et al., Biomarker detection for disease diagnosis using cost-effective microfluidic platforms, Analyst 140 (2015) 7062–7081.
[36] M. Dou, S.T. Sanjay, D.C. Dominguez, P. Liu, F. Xu, X. Li, Multiplexed instrument-free meningitis diagnosis on a polymer/paper hybrid microfluidic biochip, Biosens. Bioelectron. 87 (January 15) (2017) 865–873.
[37] A.K. Yetisen, M.S. Akram, C.R. Lowe, Paper-based microfluidic point-of-care diagnostic devices, Lab Chip 13 (June 21) (2013) 2210–2251.
[38] M. Dou, D.C. Dominguez, X. Li, J. Sanchez, G. Scott, A versatile PDMS/paper hybrid microfluidic platform for sensitive infectious disease diagnosis, Anal. Chem. 86 (August 5) (2014) 7978–7986.
[39] R. Pelton, Bioactive paper provides a low-cost platform for diagnostics, Trac-Trends in Analytical Chemistry 28 (September) (2009) 925–942.
[40] J. Hu, S. Wang, L. Wang, F. Li, B. Pingguan-Murphy, T.J. Lu, et al., Advances in paper-based point-of-care diagnostics, Biosens. Bioelectron. 54 (April 15) (2014) 585–597.
[41] A.W. Martinez, S.T. Phillips, G.M. Whitesides, E. Carrilho, Diagnostics for the developing world: microfluidic paper-based analytical devices, Anal. Chem. 82 (January 1) (2010) 3–10.
[42] C.A. Holstein, A. Chevalier, S. Bennett, C.E. Anderson, K. Keniston, C. Olsen, et al., Immobilizing affinity proteins to nitrocellulose: a toolbox for paper-based assay developers, Anal. Bioanal. Chem. 408 (Febuary) (2016) 1335–1346.
[43] M. Dou, D.C. Dominguez, X. Li, J. Sanchez, G. Scott, A versatile PDMS/Paper hybrid microfluidic platform for sensitive infectious disease diagnosis, Anal. Chem. 86 (2014) 7978–7986 2014/08/05.
[44] M. Dou, S.T. Sanjay, D.C. Dominguez, P. Liu, F. Xu, X. Li, Multiplexed instrument-free meningitis diagnosis on a polymer/paper hybrid microfluidic biochip, Biosens. Bioelectron. 87 (2017) 865–873 1/15/.
[45] P. Zuo, X. Li, D.C. Dominguez, B.-C. Ye, A PDMS/paper/glass hybrid microfluidic biochip integrated with aptamer-functionalized graphene oxide nano-biosensors for one-step multiplexed pathogen detection, Lab Chip 13 (2013) 3921–3928.
[46] G.L. Fu, S.T. Sanjay, M.W. Dou, X.J. Li, Nanoparticle-mediated photothermal effect enables a new method for quantitative biochemical analysis using a thermometer, Nanoscale 8 (2016) 5422–5427.
[47] K.S. Prasad, C. Walgama, S. Krishnan, Enhanced electroactivity and substrate affinity of microperoxidase-11 attached to pyrene-linkers pi-pi stacked on carbon nanostructure electrodes, RSC Adv. 5 (2015) 11845–11849.
[48] M. Chirea, C.M. Pereira, F. Silva, Catalytic effect of gold nanoparticles self-assembled in multilayered polyelectrolyte films, J. Phys. Chem. C 111 (2007) 9255–9266 2007/07/01.
[49] N.G. Tsierkezos, M. Puschner, U. Ritter, A. Knauer, L. Hafermann, J.M. Köhler, Electrochemical response of nitrogen-doped multi-walled carbon nanotubes decorated with gold and iridium nanoparticles toward ferrocyanide/ferricyanide redox system, Ionics 22 (October 01) (2016) 1957–1965.
[50] X.H. Huang, M.A. El-Sayed, Gold nanoparticles: optical properties and implementations in cancer diagnosis and photothermal therapy, J. Adv. Res. 1 (January) (2010) 13–28.
[51] S. Kumar, J. Aaron, K. Sokolov, Directional conjugation of antibodies to nanoparticles for synthesis of multiplexed optical contrast agents with both delivery and targeting moieties, Nat. Protoc. 3 (2008) 314–320.
[52] P. Mukherjee, R. Bhattacharya, N. Bone, Y.K. Lee, C.R. Patra, S. Wang, et al., Potential therapeutic application of gold nanoparticles in B-chronic lymphocytic leukemia (BCLL): enhancing apoptosis, J. Nanobiotechnology 5 (May 8) (2007) 4.
[53] M. Hu, J. Yan, Y. He, H. Lu, L. Weng, S. Song, et al., Ultrasensitive, multiplexed detection of cancer biomarkers directly in serum by using a quantum dot-based microfluidic protein chip, ACS Nano 4 (2009) 488–494.
[54] M. Dou, J. Sanchez, H. Tavakoli, J. E. Gonzalez, J. Sun, J. D. Bard, et al., A Low-Cost Microfluidic Platform for Rapid and Instrument-Free Detection of Whooping Cough, Anal Chim Acta, p. In Press. DOI: 10.1016/j.aca.2019.03.001, 2019 /03/05/ 2019.
[55] X. Wei, W. Zhou, S.T. Sanjay, J. Zhang, Q. Jin, F. Xu, et al., Multiplexed Instrument-Free Bar-Chart SpinChip Integrated with Nanoparticle-Mediated Magnetic Aptasensors for Visual Quantitative Detection of Multiple Pathogens, Anal. Chem. 90 (2018) 9888–9896 2018/08/21.
[56] G. Fu, S.T. Sanjay, W. Zhou, R.A. Brekken, R.A. Kirken, X. Li, Exploration of nanoparticle-mediated photothermal effect of TMB-H2O2 colorimetric system and its application in a visual quantitative photothermal immunoassay, Anal. Chem. 90 (2018) 5930–5937 2018/05/01.
[57] G. Fu, S.T. Sanjay, M. Dou, X. Li, Nanoparticle-mediated photothermal effect enables a new method for quantitative biochemical analysis using a thermometer, Nanoscale 8 (2016) 5422–5427.
[58] E. Asadian, M. Ghalkhani, S. Shahrokhian, Electrochemical sensing based on carbon nanoparticles: a review, Sens. Actuators B Chem. 293 (2019) 183–209 2019/08/15/.
[59] W.R. Jin, X.J. Li, N. Gao, Simultaneous determination of tryptophan and glutathione in individual rat hepatocytes by capillary zone electrophoresis with electrochemical detection at a carbon fiber bundle-Au/Hg dual electrode, Anal. Chem. 75 (August) (2003) 3859–3864.
[60] X.J. Li, W.R. Jin, Q.F. Weng, Separation and determination of homovanillic acid and vanillylmandelic acid by capillary electrophoresis with electrochemical detection, Anal. Chim. Acta 461 (June) (2002) 123–130.

K. Sudhakara Prasad received his Ph.D. from National Chung-Hsing University, Taiwan, in 2009. Then he carried out his postdoctoral research with Prof. Xiujun Li at University of Texas at El Paso, USA. Currently, he is an Assistant Professor at Yenepoya University, India. His research interests include electrochemical sensing and low-cost bioanalysis.

Xiyue Cao received his Master's degree from Qingdao University, China, in 2017. He is a visiting Ph.D. student from Qingdao University in Prof. Xiujun Li's group at University of Texas at El Paso. His research is focused on biosensors, electrochemistry, and nano-materials.

Ning Gao received her Ph.D. degree in Bioanalytical Chemistry and B.S. degree in Applied Chemistry from Shandong University. After completing her Ph.D., she worked on electronic sensors at Harvard University, fluorescence sensors at MIT, and controlled drug release and targeted cancer therapy at Stevens Institute of Technology. She has extensive expertise in bioelectronics, advanced manufacturing, surface chemistry, materials science, and biomedical engineering.

Qijie Jin is a Ph.D candidate in Nanjing Tech University. His research interests include environmental science and engineering.

Sanjay Sharma Timilsina from Nepal received his master's degrees in biotechnology from Bangalore University, India in 2012, and then worked with Prof. XiuJun Li in the Department of Chemistry at University of Texas at El Paso in USA for his Ph.D. study. He received his Ph.D. degree from University of Texas at El Paso in 2018. His research interest is focused on low-cost diagnosis of infectious diseases on microfluidic platforms. He is also interested in 3D cell culture and bioanalysis.

Gilberto Henao-Pabon is a Ph.D. student in the Biomedical Engineering program in Prof. Xiujun Li's group at University of Texas at El Paso. His research interests include low-cost disease diagnosis, electrochemical analysis, and paper-based microfluidics.

XiuJun (James) Li received his Ph.D. in bioanalytical chemistry in 2008 from Simon Fraser University, Canada, and then moved to University of California Berkeley and Harvard University for his postdoctoral research from 2009 to 2011, as an NSERC Postdoctoral Fellow. Currently, he is a tenured Associate Professor in the Department of Chemistry & Biochemistry, Biomedical Engineering (BME), Border Biomedical Research Center (BBRC), and Environmental Science & Engineering (ESE) at University of Texas at El Paso (UTEP), USA. His current research interest is focused on bioanalysis, bioengineering, and environmental science & engineering using microfluidic lab-on-a-chip and nanotechnology, including but not limited to low-cost diagnosis, hybrid microfluidic devices, nano-biosensing, single-cell analysis, and 3D cell culture.